Impacts of Inverter-Interfaced Wind Power Plants in the Phase-Selection and Directional Protection Functions

Moisés J. B. B. Davi (iD), Mário Oleskovicz (iD), Felipe V. Lopes (iD), *Senior Member, IEEE*, and David C. Jorge (iD)

Abstract—Considering the increasing insertion of Inverter-Interfaced Wind Power Plants (IIWPP) in modern power systems, this paper evaluates the impacts of this generation type on directional and phase selection functions. Six algorithms not yet explored in the context of IIWPP were evaluated, considering Full-Converter (FC) and Doubly-Fed Induction Generator (DFIG) topologies. For the studies, an IIWPP was modeled in detail using the Matlab/Simulink software. Contingency scenarios varying the type, resistance, and fault location have been simulated on a transmission line that connects the IIWPP to the primary grid. Thus, it was possible to report in detail the operational particularities of IIWPP that impact such functions, besides providing recommendations about the characteristics that these algorithms should contemplate to satisfactorily operate in systems with the presence of FC and DFIG generators.

Index Terms—DFIG, Full-Converter, Protection Functions, Renewable Energy, Wind Turbine.

I. INTRODUCTION

In the last years, wind generations are becoming increasingly important in the energy scenario of modern electrical systems. Among the various wind power generation topologies [1], the Full-Converter (FC) and Doubly-Fed Induction Generator (DFIG) have aroused the concern of researchers in the electrical sector because they present atypical operational behavior, when compared to conventional generations [1].

Historically, the Inverter-Interfaced Wind Power Plants (IIWPP) account for a relatively low percentage of the power system generation capacity, and therefore such generations used to be quickly disconnected under grid disturbance conditions. However, with the growing penetration of IIWPP in electrical power systems, the loss of this large generation portion during disturbances has become a critical condition from a system stability perspective. Then, several countries have adopted requirements for these generations to have the capability, called Fault Ride-Through (FRT), to stay connected even if the grid is in disturbing situations [2]. With such requirements, the analysis of the fault contributions of IIWPP has been the focus of several researchers in the last years [3]–[8], mainly after evidence of protection misoperations have been reported. Considering that most of the larger renewable power plants are connected to transmission and sub-transmission systems, some

studies about the interaction between IIWPP and distance protection have been conducted [9], [10].

Studies of misoperations due to errors in phase-selection and directional algorithms have also been conducted. However, most of the publications on this topic restrict the analysis to FC generators, evaluating few algorithms for the directional functions in some works [11], [12] and phase-selection functions in others [13], [14]. The impact of DFIG topology generations is considered in [15]. However, analyzing misoperations only for directional functions upon three-phase faults in the system. The studies performed in [16] consider both FC and DFIG topologies, but the authors evaluate only directional algorithms, while in [17], [18], only protection schemes based on negative sequence components are assessed.

Thus, this paper aims to contribute to the literature by bringing analyses of six directional and phase-selection algorithms not yet explored in the context of IIWPP, considering both FC and DFIG topologies, and presenting the obtained waveforms to concisely clarify the atypical characteristics of IIWPP that result in misoperations by such functions. The analyzed waveforms are obtained from simulations that contemplate detailed FC and DFIG generation topologies and the traditional topology for the interconnection of wind power plants to the grid. For the studies, contingency scenarios varying the type, resistance, and fault location have been simulated on a transmission line (TL) that connects the IIWPP to the primary grid. Thus, it was possible to report several IIWPP operational particularities that impact directional and phase-selection functions, besides providing recommendations about the characteristics that such algorithms should cover to satisfactorily operate in systems with IIWPP.

II. FAULT CONTRIBUTIONS OF DFIG AND FC GENERATIONS

Regarding the analysis of fault contributions, in systems with conventional generators, the generators can be represented as sources in series with impedances. In contrast, for IIWPP, the fault contributions are governed by the converter control systems, which can be quite diverse depending on the manufacturer, making the analysis complex [1].

FCG typically consists of a synchronous generator, a turbine, and an AC-DC-AC converter [1]. Due to the thermal limits of the converter's devices, the fault contributions of these generations are limited to shallow levels (typically up to 1.2 p.u. [1]), with behavior varying according to the converter's control methods. Among these methods, the Coupled

Sequence Control (CSC) is widely applied [19], whereby the fault contributions contemplate only the positive-sequence current, even under unbalanced fault conditions. Another control scheme is the Decoupled Sequence Control (DSC) [4], [19], [20], whereby under asymmetrical faults, the converters of IIWPP are controlled to emulate conventional generator characteristics concerning the negative sequence contributions.

DFIG, in turn, operates with the same principles as conventional induction generators with the particularity that it can work with larger slips, typically limited to ±30% [9]. The machine's stator winding is powered directly by the grid voltage, leading their fault currents to present higher levels (typically up to 2 p.u. [1]) compared to FCG [6], [21]. Furthermore, considering that the traditional CSC controls the converters, it is expected that, under unbalanced fault conditions, the DFIG generation promotes the injection of the negative sequence current, differently from what occurs in FC generation. However, it is worth mentioning that other control methodologies allow, for the DFIG topology under unbalanced faults, the suppression of the negative sequence current, aiming to improve its transient performance [18].

It is pointed out that the IIWPP controls can be divided into two main approaches: Grid-Following (GFL) and Grid-Forming (GFM) [7]. Despite several recent studies on the application of GFM control [5], [7], in transmission systems, the IIWPPs' converters are of the GFL approach typically, where a phase-locked loop is used for tracking the grid angle and frequency to control the active and reactive powers supplied by IIWPPs [7]. Therefore, the GFL approach was employed for all the analyses performed in this paper.

III. TEST SYSTEM FOR THE STUDIES

The test system single-line diagram and parameters are illustrated in Fig. 1 and Table I, respectively. The proposed system was modeled in MATLAB software using the Simulink toolbox. The simulations performed were of the discrete type, using a fixed integration step of 5 μs and the Tustin/Backward Euler solution method available in the software. The system includes a source in series with an impedance representing the grid, with a voltage level of 500 kV and 60 Hz frequency. The wind farm (WF) connection to the grid is made by a 239 km TL, represented in this case by distributed parameters and the Bergeron model. Power transformers responsible for raising the voltage from generation levels to sub-transmission (delta-star connection) and finally to the transmission levels (star-star connection) were also represented. Each wind turbine is connected to the medium voltage system by a transformer (Dyn11 - 34.5/0.575 kV - Z = 6%) with a power of 1.75 MVA.

For modeling the FC generators, synchronous machines were used, and all controls were set as described in [22], [23]. The DC link consists of a 0.09 Farad capacitor with a nominal voltage of 1100 V. The coupling choke circuit has a resistance of 0.003 p.u. and an inductance of 0.15 p.u. at the machine base, and the RC output filter has a power of 120 kvar. The Chopper circuit was designed to operate when the DC link voltage exceeds 1.1 p.u.. It is disabled when this voltage reaches values below 1.08 p.u.. The nominal data for
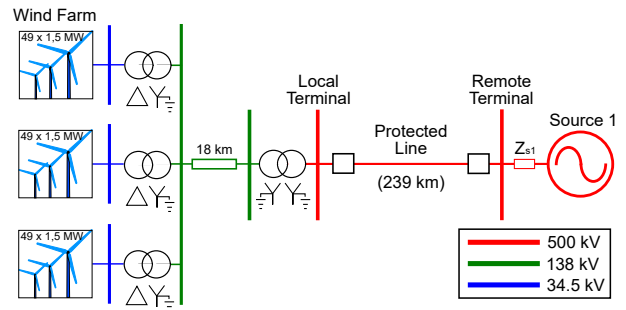

Fig. 1. Proposed system single-line diagram.

TABLE I
PROPOSED SYSTEM PARAMETERS.

Parameters	Value
Equivalent System	500 kV - 10 GVA - X/R = 10
Transmission Line (239 km)	R+/0 = 0.019/0.204 ohm/km L+/0 = 0.818/2.170 mH/km C+/0 = 0.014/0.009 μF/km
Transformer YNyn0 500 – 138 kV	360 MVA - Z = 10%
Feeder (18 km)	R = 0.191 ohm/km L = 1.192 mH/km
Transformers YNd1 138 - 34.5 kV	90 MVA - Z = 10%

the synchronous generators are: S_n = 1.67 MVA, V_n = 730 V, R_s = 0.006 p.u., X_l = 0.18 p.u., X_d = 1.305 p.u., X_d' = 0.296 p.u., X_d'' = 0.252 p.u., X_q = 0.474 p.u., X_q'' = 0.243 p.u., T_{do}' = 4.49 s, T_{do}'' = 0.0681 s, and T_q'' = 0.0513 s.

To model DFIG unit, all controls were adjusted as described in [23], [24]. The DC link consists of a 0.01 Farad capacitor with a nominal voltage of 1150 V. The coupling choke circuit has a resistance of 0.003 p.u. and inductance of 0.3 p.u. at the machine base, and the RC output filter has a power of 120 kvar. The Chopper circuit was designed to operate when the DC link voltage exceeds 1.1 p.u.. It is disabled when this voltage reaches values below 1.08 p.u.. The crowbar circuit was designed to operate when the measured rotor current exceeds 4 p.u. or when the DC link voltage exceeds 1.2 p.u.. It is kept active for a total time of 60 milliseconds after its operation. The nominal data for the induction generators are: S_n = 1.67 MVA, V_n = 575 V, R_s = 0.023 p.u., R_r = 0.016 p.u., X_m = 2.9 p.u., X_s = 0.18 p.u., and X_r = 0.16 p.u.

For comparison purposes and study of the main IIWPP, some scenarios were simulated considering the FC topology, and others considering DFIG. In both cases, the active and reactive powers supplied by the generating units to the grid are controlled at 220 MW and 0 var, respectively. Concerning the converter controls, the traditional CSC [19] was considered for both topologies. Short-circuits in the 239 km TL were simulated, varying the fault type (Single-phase-to-ground – AG, Two-phase - AB, Two-phase-to-ground - ABG, and Three-phase - ABC), fault resistance (0 Ω, 50 Ω, and 100 Ω), and fault location (10%, 30%, 50%, 70%, and 90% of the TL, being 0% the remote terminal). Then, considering FC and

DFIG topologies, a total of 120 cases were simulated.

Considering the simulated scenarios, case studies about misoperations of phase-selection and directional functions were performed.

IV. CURRENT ANGLE-BASED PHASE-SELECTION ALGORITHMS

In the current angle-based phase-selection algorithms, the fault type is determined by the following steps [25]:

1) Determination of positive, negative, and zero sequence currents based on the monitored phase currents;
2) Accurate estimation of sequence current's phase angles;
3) Calculation of the phase shifts between the negative and zero or negative and positive sequence currents, depending on the chosen method;
4) Assuming that the sequence currents are measured with reference in phase A, define the fault type based on the sequence current phase shifts and the regions illustrated in Fig.2 and defined in Table II.

The method based on the zero and negative sequence current angles (Fig.2-a) can not distinguish between single-phase or two-phase-to-ground faults. Therefore, the method based on the positive and negative sequence currents (Fig.2-b) can be used to complement it by distinguishing between a single-phase and a two-phase fault. The monitoring of the zero-sequence component can also be used to distinguish between faults that do or do not involve ground. Moreover, it is typically used the incremental positive sequence current for the algorithm evaluation to avoid the influence of load currents on phase-selection [25].
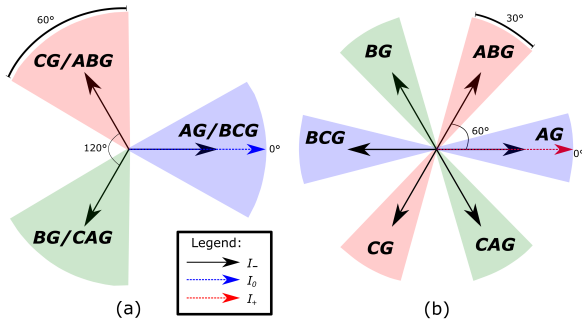

Fig. 2. Phase-selection algorithm by (a) zero (I_0) and negative (I_-) or (b) positive (I_+) and negative sequence currents [25].

TABLE II
PHASE SHIFTS BETWEEN THE SEQUENCE CURRENTS [25].

(a) Using $\angle\overrightarrow{I_-}$ and $\angle\overrightarrow{I_0}$		(b) Using $\angle\overrightarrow{I_-}$ and $\angle\overrightarrow{I_+}$	
Fault Type	$(\angle\overrightarrow{I_-} - \angle\overrightarrow{I_0})$	Fault Type	$(\angle\overrightarrow{I_-} - \angle\overrightarrow{I_+})$
AG	]-60°, 60°[	AG	]-30°, 30°[
BG	]180°, 300°[	BG	]90°, 150°[
CG	]60°, 180°[	CG	]210°, 270°[
AB/ABG	]60°, 180°[	ABG	]30°, 90°[
BC/BCG	]-60°, 60°[	BCG	]150°, 210°[
CA/CAG	]180°, 300°[	CAG	]270°, 330°[

A. Results and Discussions

In order to demonstrate the misoperation cases on current angle-based phase-selection algorithms, the results for AG and ABG faults, at 50% of the protected TL, and without resistance, will be shown and discussed. The faults were started at instant t = 1.1 seconds. Figs. 3 and 4 show the magnitudes and angles of the sequence currents (I_{seq+}, I_{seq-}, I_{seq0}), measured at the remote and local terminals (for both DFIG and FC generations), for the scenarios considering the
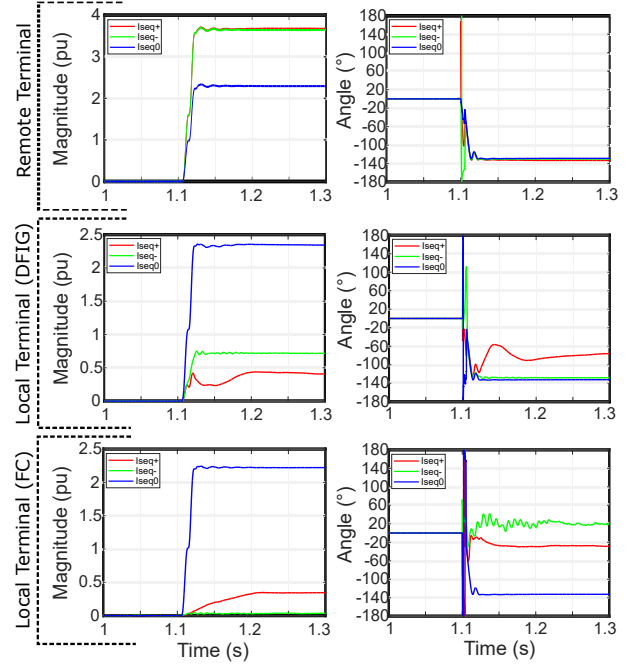

Fig. 3. Monitored current magnitudes and angles for AG fault (DFIG and FC generations).
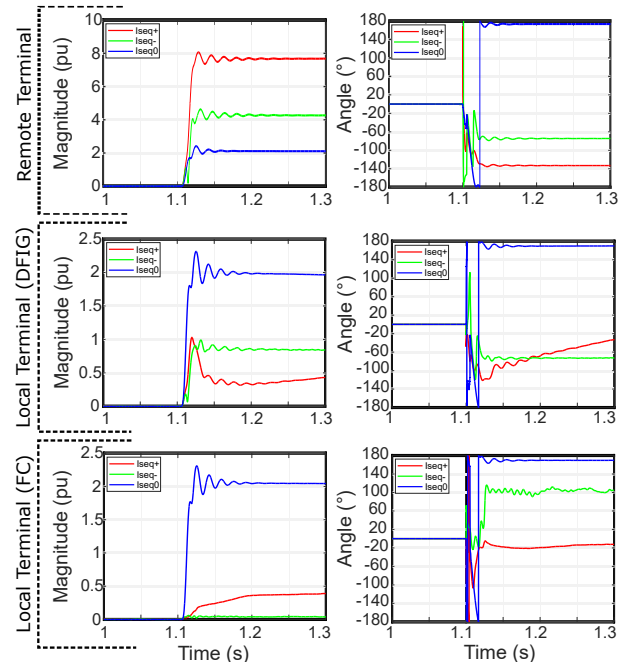

Fig. 4. Monitored current magnitudes and angles for ABG fault (DFIG and FC generations).

AG and ABG faults, respectively.

For the scenario considering the AG fault, regarding the measurements at the remote terminal, the typical characteristics were obtained, i.e., a high magnitude for the positive (3.6 p.u.), negative (3.6 p.u.), and zero (2.3 p.u.) sequence currents during the fault. It is also observed that the positive, negative, and zero sequence currents are practically in-phase (-128.8°), resulting in the satisfactory operation of the phase-selection algorithm exposed in this work, indicating an AG fault by the positive/negative sequence algorithm and an AG or BCG fault by the zero/negative sequence algorithm.

Through the analysis of the local terminal measurements, considering the IIWPP with DFIG topology, it can be concluded that the magnitude of the positive (0.4 p.u.) and negative (0.7 p.u.) sequence currents were significantly reduced if compared to the remote terminal measurements, evidencing the current limiting characteristics by the converter controls. The zero-sequence current magnitude (2.3 p.u.) was the highest because in this case, the zero-sequence contribution from the remote terminal flows through the local terminal via the neutral point of the 500 kV transformer. For the current angles, the negative and zero sequence components are practically in-phase (-128.2°), while the positive sequence component, in the initial instants of fault, assumes values close to -111°, and such value tends to increase, assuming -76.6° after the 300 milliseconds of simulated fault. This variable characteristic is due both to the inverter controllers' action and the demagnetization of the induction machine after the significant reduction of its terminal voltage. In this context, it can be concluded that the phase-selection algorithm based on the zero/negative sequence currents would result in the indication of an AG or BCG fault. In contrast, the algorithm based on the positive/negative sequence currents would indicate an AG type fault in the initial fault instants, tending to the indication of an AC or ACG type after the initial fault instants.

Finally, through the analysis of the local terminal measurements, considering the IIWPP with FC topology generators, it can be concluded that the magnitude of the positive sequence current (0.3 p.u.) was significantly reduced, and the zero-sequence current magnitude (2.3 p.u.) was the highest, as observed for the DFIG topology. It can also be observed that the negative sequence component had its magnitude almost totally suppressed (0.03 p.u.), being this a typical characteristic of converter CSC adopted in the simulations of this paper [19]. For the current angles, the negative sequence component leads the positive sequence by approximately 51.1° and the zero-sequence by 109.1°. Therefore, the algorithm based on the zero/negative sequence components indicates a CG or ABG fault, while the algorithm based on the positive/negative sequence components would indicate an AB or ABG fault.

For the scenario considering the ABG fault, the obtained results were similar, since it is observed: (1) correct algorithm phase-selections for remote terminal measurements; (2) misoperations for the algorithm based on the positive/negative sequence currents, after some milliseconds of fault for the DFIG topology; (3) improper performances for the FC topology justified by the adoption of the CSC in this work.

For the simulated two-phase faults without ground involve-ment, the conclusions are the same as for two-phase-to-ground faults, except for the conclusions related to zero-sequence components that are non-existent for this fault type. The variation of the fault location affected in a more significant way the current magnitudes, slightly interfering in the angular phase shifts between the current sequence components. Finally, the variation of the fault resistance affected both the magnitude and angle of the measured currents. However, the conclusions about the algorithm misoperations were similar, being the angles of the positive and zero sequence components the most affected, as expected.

B. Highlights and Recommendations

The performed analyses show that the algorithm based on the positive/negative sequence components was effective only for the remote terminal measurements. In contrast, the algorithm based on the zero/negative sequence components was adequate for local and remote terminal measurements when the WF generators are of the DFIG topology. For the initial fault instants, the algorithm based on the positive/negative sequence components was also effective for DFIG topology. Regarding the compromise of the current angle-based algorithms, it is recommended that for applications involving IIWPP, the selection of phases under fault be performed with algorithms based not only on the currents but also on the voltages [13]. So, avoid using the negative sequence currents, especially in WF with FC generators. This recommendation is made based on the fact that the measured sequence voltage angles at both terminals of the protected TL were quite similar in all performed tests.

V. CURRENT MAGNITUDE-BASED PHASE-SELECTION ALGORITHMS

In the current magnitude-based phase-selection algorithms, the fault type is determined by the following steps [26]:

1) Calculation of phase-to-phase (PP) loop currents I_{ab}, I_{bc}, and I_{ca};
2) Determination of superimposed currents (ΔI_{ab}, ΔI_{bc}, and ΔI_{ca}) by subtracting the present and two cycles' previous values of the PP loop currents;
3) Define the fault type based on the expected levels for the superimposed current for each fault type, as defined in Table III.

For the analyses performed in this paper, the maximum measured superimposed current was adopted as the reference and assumed as a high-level signal, and the definition of high or low level for the other currents will be made based on the threshold of 80% of the maximum current [26].

TABLE III
LEVELS OF SUPERIMPOSED CURRENTS [26].

	AG	BG	CG	AB	BC	CA	ABC
ΔI_{ab}	High	High	Low	High	Low	Low	High
ΔI_{bc}	Low	High	High	Low	High	Low	High
ΔI_{ca}	High	Low	High	Low	Low	High	High

A. Results and Discussions

To demonstrate misoperations in the current magnitude-based phase-selection algorithm, the results for AG and ABG faults, at 50% of the protected TL, and without resistance, will be shown. The faults were started at instant t = 1.1 seconds. For such scenarios, the superimposed currents (ΔI_{ab}, ΔI_{bc}, ΔI_{ca}) measured at the remote and local terminals (DFIG and FC generations) are illustrated in Fig. 5.

The results obtained with the AG fault, exposed in Fig. 5-a, show that the superimposed currents measured at the remote terminal indicate the occurrence of an AG fault since the ΔIab and ΔIca currents assumed high levels (approximately 6 p.u.), while ΔIbc remained at very low levels. About the superimposed currents measured at the local terminal for DFIG generations at the WF, it is first observed that the obtained values are significantly lower than those obtained at the remote terminal (maximum values of approximately 0.98 p.u.). However, it is also observed that the ΔIab and ΔIca currents assumed higher levels compared to the ΔIbc current level (approximately 56% of the ΔIab and ΔIca values), thus indicating the occurrence of an AG fault by the algorithm. Finally, for FC generations in the WF, very low levels of superimposed currents were obtained (of approximately 0.2 p.u. after the initial cycles), and only in the first cycle after the fault inception, the ΔIab and ΔIca currents are observed with higher values, which would result in the indication of an AG fault type. After the initial cycle, it is noticed that the currents tend to assume very similar values, which would indicate an ABC fault by the selection algorithm.

Concerning the obtained results with the simulation of ABG faults, Fig. 5-b shows that the superimposed currents measured at the remote terminal indicate the occurrence of an ABG fault since the ΔIab current assumed the highest level (16.8 p.u.), followed by ΔIbc (10.2 p.u., equivalent to 60% of the maximum value) and, finally, of ΔIca (8.1 p.u., equivalent to 48% of the maximum value). For the superimposed currents measured at the local terminal for DFIG generations in the WF, a significant reduction in the obtained values is also observed (maximum values of approximately 2.69 p.u.). However, similarly to what was noted for the remote terminal measurements, the ΔIab current assumed the highest level (2.69 p.u.), followed by ΔIbc (1.41 p.u., equivalent to 52% of the maximum value) and, finally, ΔIca (1.28 p.u., equivalent to 47% of the maximum value) thus indicating the occurrence of an ABG fault by the algorithm. For FC generations in the WF, the conclusions are the same as for single-phase faults, resulting in the indication of an ABG fault type based only on the initial cycles, with the tendency to indicate an ABC fault by the similarity between the currents.

For the simulated two-phase faults without ground involvement, the conclusions are the same as for two-phase-to-ground faults. The variation of both the fault resistance and the fault location in the TL has not modified the relationships between the phase-selection quantities.

B. Highlights and Recommendations

From the performed analyses, the method's effectiveness was observed for the remote terminal measurements. Regarding local terminal measurements when considering DFIG generators at WF, the expected behavior for the superimposed currents occurred. However, the obtained levels for such currents were significantly lower, which may require relatively low minimum thresholds for sensitization of the selection method. Considering FC topology generators at the WF, it was observed that the method was effective only in the initial cycle after fault inception, when the superimposed current levels are too low, and may then return erroneous phase-selection results.

Thus, for using methods based on superimposed magnitudes in systems with IIWPP, this paper brings two main recommendations: (1) related to the low levels obtained for the superimposed currents, which can be a challenge in terms of sensitivity, methods from which the resulting superimposed quantities have higher levels are needed; (2) related to the response of the FC generation converter controls that changed the superimposed current characteristics a few cycles after the fault, resulting in misoperations, methods with responses based only on the initial cycles after the fault inception are needed.
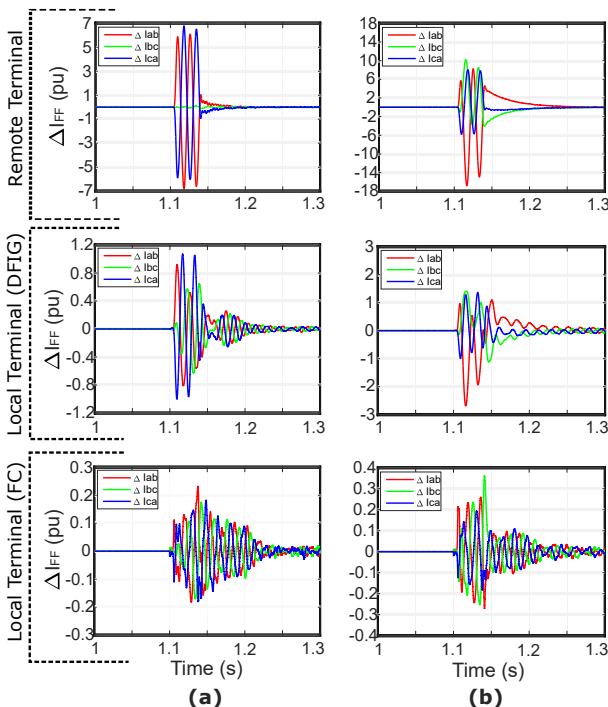
VI. TORQUE-BASED DIRECTIONAL ALGORITHMS

Regarding the directional algorithm evaluated, this is based on the Equations 1, 2 and 3, for positive (T_1), negative (T_2) and zero-sequence (T_0) elements, respectively [27].

$$T_1 = \mid 3\overrightarrow{V_1} \mid * \mid 3\overrightarrow{I_1} \mid * cos(\angle 3\overrightarrow{V_1} - \angle 3\overrightarrow{I_1} - \angle Z_{L1}) \quad (1)$$

$$T_2 = \mid 3\overrightarrow{V_2} \mid * \mid 3\overrightarrow{I_2} \mid * cos(\angle -3\overrightarrow{V_2} - \angle 3\overrightarrow{I_2} - \angle Z_{L1}) \quad (2)$$

$$T_0 = \mid 3\overrightarrow{V_0} \mid * \mid 3\overrightarrow{I_0} \mid * cos(\angle -3\overrightarrow{V_0} - \angle 3\overrightarrow{I_0} - \angle Z_{L0}) \quad (3)$$

Fig. 5. Superimposed currents for (a) AG and (b) ABG faults (DFIG and FC generations).

$\overrightarrow{V_1}$, $\overrightarrow{V_2}$, and $\overrightarrow{V_0}$ are the positive, negative and zero-sequence voltages, $\overrightarrow{I_1}$, $\overrightarrow{I_2}$ and $\overrightarrow{I_0}$ are the positive, negative and zero-sequence currents, and Z_{L1} and Z_{L0} are the TL positive and zero-sequence impedances. The torque signal will be positive for forward faults and negative for reverse faults [27].

The negative sequence directional function is the most widely used to identify the direction of asymmetrical faults. The positive sequence directional function is typically employed when the negative sequence component is unreliable. Regarding the zero-sequence directional element, although this is used in some relays, it cannot identify non-grounded faults.

The analyses performed in this paper were based on the cosine function argument of the Equations 1, 2 and 3, resulting in angles between +90° and -90°, indicating a fault in the direct region, i.e., within the TL.

A. Results and Discussions

Aiming to demonstrate misoperations in the torque-based directional algorithm, the results for AG and ABG faults, at 50% of the protected TL, and without resistance, will be shown. The faults were started at instant t = 1.1 seconds. For such analysis, the torque angles (T_{seq+}, T_{seq-}, T_{seq0}) that are arguments of the cosine function in Equations 1, 2 and 3, obtained from measurements at the remote and local terminals (DFIG and FC generations), are illustrated in Fig. 6.

For the AG fault scenario, illustrated in Fig. 6-a, it is observed that for the remote terminal measurements, the resulting torque angles for all sequences are very close to 0°, indicating the fault in the direct region. Regarding the measurements at the local terminal for DFIG generations at WF, the torque angles for all sequences are in the zone indicating the fault in the direct region. However, it is worth mentioning that the

positive sequence torque angle is very close to the threshold between the direct and reverse zone (angle of approximately -80°). Finally, for the measurements at the local terminal for FC generations in the WF, the fault indication in the direct region occurred only for the zero-sequence component, being the positive sequence torque angle of approximately -95° and that of the negative sequence component of the -148°.

Considering the ABG fault scenario, illustrated in Fig. 6-b, it is observed that for the remote terminal measurements, the resulting torque angles for all sequences are also very close to 0°, indicating the fault in the direct region. For the measurements at the local terminal considering DFIG generations at WF, the torque angles of the negative and zero sequences are in the zone indicating the fault in the direct region. However, the positive sequence torque angle is within the direct zone only in the initial fault instants, reaching the reverse zone after the 300 milliseconds of simulated fault. Finally, for the measurements at the local terminal for FC generations in the WF, the fault indication in the direct region occurred again only for the zero-sequence component, being the positive sequence torque angle of approximately -95° and that of the negative sequence component of the ±180°.

For the simulated two-phase faults without ground involvement, the conclusions are the same as for two-phase-to-ground faults, except for the conclusions related to zero-sequence components that are non-existent for this fault type. The variation of the fault location did not affect the measured angles significantly, and consequently, the conclusions about the operation of the directional algorithm are the same. Finally, by varying the fault resistance value, more significant variations were verified for the positive sequence component, with similar conclusions about the algorithm misoperations.

B. Highlights and Recommendations

Through the analyses carried out, it was observed that the algorithm returned a direct fault indication for all the tests performed with the remote terminal measurements, as expected. The algorithm that relates the zero-sequence component angles was effective for the measurements performed at the local terminal. In contrast, the algorithm that relates the negative sequence component angles was effective only for the DFIG generation, indicating a fault in the reverse region for all tests with the FC generation. Finally, for the algorithm that relates the positive sequence component angles, in the scenarios with DFIG generation, it was effective only on the initial cycles after the fault inception. For the scenarios with FC generation, no effectiveness has been found.

Therefore, it is recommended that for systems with IIWPP, the use of the zero-sequence directional element be prioritized, which operated satisfactorily for all simulated grounded faults. For situations where the zero-sequence component is not feasible or possible, the negative sequence component can be used, if it is not suppressed on the methodology adopted for the converter controls [19]. If the negative sequence component is suppressed after the response of the converter controls, it is recommended to use methods with a response time shorter than that of the converter controls, avoiding misoperations. In [11], a method with a shorter response time is presented.
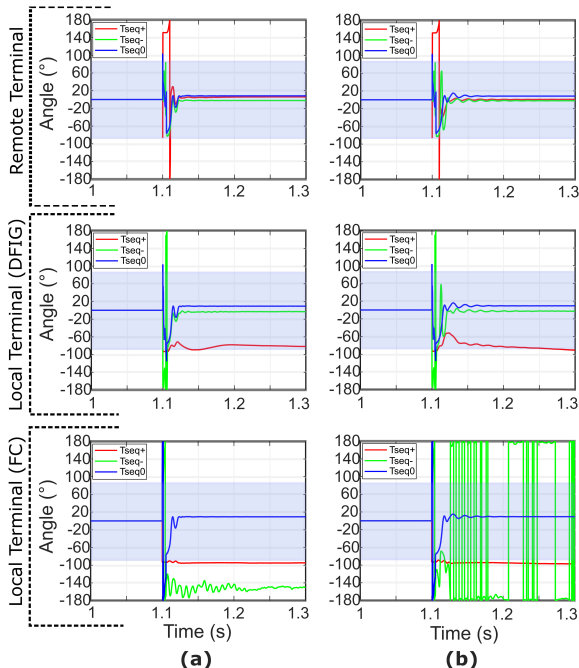

Fig. 6. Torque angles for (a) AG and (b) ABG faults (DFIG and FC generations).

VII. Conclusions

This paper presented case studies to show the impact of the atypical characteristics of FC and DFIG generations on the phase-selection and directional functions, not yet explored in the context of IIWPP. Besides providing theoretical explanations for the misoperations of directional and phase-selection functions, this paper contemplated recommendations about the characteristics that these algorithms should attend to satisfactorily operate in systems with IIWPP.

Acknowledgment

References

[1] K. Jones *et al.*, "Impact of inverter based generation on bulk power system dynamics and short-circuit performance," 07 2018.

[2] P. Piya, M. Ebrahimi, M. Karimi-Ghartemani, and S. A. Khajehoddin, "Fault ride-through capability of voltage-controlled inverters," *IEEE Trans. on Industrial Electr.*, vol. 65, no. 10, pp. 7933–7943, 2018.

[3] T. Bi, B. Yang, K. Jia, L. Zheng, Q. Liu, and Q. Yang, "Review on renewable energy source fault characteristics analysis," *CSEE Journal of Power and Energy Systems*, vol. 8, no. 4, pp. 963–972, 2022.

[4] Q. Zhang, D. Liu, Z. Liu, and Z. Chen, "Fault modeling and analysis of grid-connected inverters with decoupled sequence control," *IEEE Trans. on Industrial Electr.*, vol. 69, no. 6, pp. 5782–5792, 2022.

[5] M. Habibullah, F. Gonzalez-Longatt, M. N. Acosta Montalvo, H. R. Chamorro, J. L. Rueda, and P. Palensky, "On short circuit of grid-forming converters controllers: A glance of the dynamic behaviour," in *2021 IEEE PES ISGT Latin America*, pp. 1–5, 2021.

[6] F. Jiménez-Buendía, A. Honrubia-Escribano, A. Lorenzo-Bonache, E. Artigao, and E. Gómez-Lázaro, "Short-circuit current contribution of doubly-fed wind turbines according to iec and ieee standards," *IEEE Transactions on Power Delivery*, vol. 36, no. 5, pp. 2904–2912, 2021.

[7] C. Collados-Rodriguez, M. Cheah-Mane, F.-J. Cifuentes-Garcia, E. Prieto-Araujo, and O. Gomis-Bellmunt, "Grid-following and grid-forming converter control comparison under fault conditions," in *2021 IEEE 12th ECCE-Asia*, pp. 598–603, 2021.

[8] K. Jia, Q. Liu, B. Yang, L. Zheng, Y. Fang, and T. Bi, "Transient fault current analysis of iiress considering controller saturation," *IEEE Transactions on Smart Grid*, vol. 13, no. 1, pp. 496–504, 2022.

[9] A. Hooshyar, M. A. Azzouz, and E. F. El-Saadany, "Distance protection of lines connected to induction generator-based wind farms during balanced faults," *IEEE Transactions on Sustainable Energy*, vol. 5, no. 4, pp. 1193–1203, 2014.

[10] A. Hooshyar, M. A. Azzouz, and E. F. El-Saadany, "Distance protection of lines emanating from full-scale converter-interfaced renewable energy power plants—part i: Problem statement," *IEEE Transactions on Power Delivery*, vol. 30, no. 4, pp. 1770–1780, 2015.

[11] K. Jia, Y. Zhe, Y. Fang, T. Bi, and M. Sumner, "Influence of inverter-interfaced renewable energy generators on directional relay and an improved scheme," *IEEE Trans. on Power Electr.*, pp. 1–1, 03 2019.

[12] B. Chen, A. Shrestha, F. A. Ituzaro, and N. Fischer, "Addressing protection challenges associated with type 3 and type 4 wind turbine generators," in *2015 68th Annual Conference for Protective Relay Engineers*, pp. 335–344, 2015.

[13] A. Hooshyar, E. F. El-Saadany, and M. Sanaye-Pasand, "Fault type classification in microgrids including photovoltaic dgs," *IEEE Transactions on Smart Grid*, vol. 7, no. 5, pp. 2218–2229, 2016.

[14] M. Azzouz, A. Hooshyar, and E. El-Sadany, "Resilience enhancement of microgrids with inverter-interfaced dgs by enabling faulty phase selection," *IEEE Transactions on Smart Grid*, vol. PP, pp. 1–1, 06 2017.

[15] A. Hooshyar, M. A. Azzouz, and E. F. El-Saadany, "Three-phase fault direction identification for distribution systems with dfig-based wind dg," *IEEE Trans. on Sust. Energy*, vol. 5, no. 3, pp. 747–756, 2014.

[16] A. Hooshyar and R. Iravani, "A new directional element for microgrid protection," *IEEE Trans. on Smart Grid*, vol. 9(6), pp. 6862–6876, 2018.

[17] A. Haddadi *et al.*, "Impact of inverter-based resources on protection schemes based on negative sequence components," 2019.

[18] I. Erlich, T. Neumann, F. Shewarega, P. Schegner, and J. Meyer, "Wind turbine negative sequence current control and its effect on power system protection," in *2013 IEEE PES General Meeting*, pp. 1–5, 2013.

[19] T. Kauffmann *et al.*, "Short-circuit model for type-iv wind turbine generators with decoupled sequence control," *IEEE Transactions on Power Delivery*, vol. 34, no. 5, pp. 1998–2007, 2019.

[20] T. Wijnhoven, G. Deconinck, T. Neumann, and I. Erlich, "Control aspects of the dynamic negative sequence current injection of type 4 wind turbines," in *2014 IEEE PES General Meeting | Conference & Exposition*, pp. 1–5, 2014.

[21] A. El-Naggar and I. Erlich, "Fault current contribution analysis of doubly fed induction generator-based wind turbines," *IEEE Transactions on Energy Conversion*, vol. 30, no. 3, pp. 874–882, 2015.

[22] O. Tremblay, R. Gagnon, and M. Fecteau, "Real-time simulation of a fully detailed type-iv wind turbine," 07 2013.

[23] N. Miller, J. Sanchez-Gasca, W. Price, and R. Delmerico, "Dynamic modeling of ge 1.5 and 3.6 mw wind turbine-generators for stability simulations," in *2003 IEEE Power Engineering Society General Meeting (IEEE Cat. No.03CH37491)*, vol. 3, pp. 1977–1983 Vol. 3, 2003.

[24] R. Gagnon, G. Turmel, C. Larose, J. Brochu, G. Sybille, and M. Fecteau, "Large-scale real-time simulation of wind power plants into hydro-québec power system," 2010.

[25] B. Kasztenny, "Phase selection for single-pole tripping - weak infeed conditions and cross-country faults," 10 2000.

[26] P. Horton and S. Swain, "Using superimposed principles (delta) in protection techniques in an increasingly challenging power network," in *2017 70th Annual CPRE*, pp. 1–12, 2017.

[27] J. Roberts and A. Guzman, "Directional element design and evaluation," 2006.

Moisés J. B. B. Davi received his degree in Electrical Engineering (2014) and his M.Sc degree in Technological Innovation (2021) from the Federal University of Triângulo Mineiro. He has 5 years of experience in the area of electrical systems protection, IED commissioning, simulation/analysis of electromagnetic transients and oscillography analysis. He is currently a PhD student at the University of São Paulo (EESC-USP), with research in the area of system protection with converter-based generations.

Mário Oleskovicz received his degree in Electrical Engineering from the Federal University of Santa Catarina, Brazil, in 1995. He got his MSc and PhD degrees in Electrical Engineering from the São Carlos Engineering School, University of São Paulo (USP), Brazil, in 1997 and 2001, respectively. Currently, he is an Assistant Professor at the Department of Electrical and Computer Engineering, São Carlos Engineering School, University of São Paulo (USP). He works with research and projects focusing on power systems, power quality, and digital protection.

Felipe V. Lopes (SM'10) was born in Brazil, 1985. He received his B.Sc., M.Sc. and Ph.D. degrees in Electrical Engineering from Federal University of Campina Grande (UFCG), Brazil, in 2009, 2011 and 2014, respectively. From 2014 to 2021 he worked as a professor at the University of Brasília (UnB), Brazil, and in 2021, he joined the Department of Electrical Engineering at the Federal University of Paraíba (UFPB), Brazil. His research interests are electromagnetic transients, fault location and power system protection.

David Calhau Jorge received his degree in Electrical Engineering from the School of Engineering of São Carlos - USP (1993), his M.Sc. and Ph.D. degrees in Electrical Engineering from the São Carlos Engineering School, University of São Paulo (USP), in 1997 and 2003, respectively. He has worked as a professor at the University of Uberaba (7 years), State University of Maringá (2 years), Federal University of Viçosa (2 years) and is currently Associate Professor II at the Federal University of Triângulo Mineiro in Uberaba - MG.